NASA Technical Memorandum 112204

Aerothermal Performance Constraints for Hypervelocity Small Radius Unswept Leading Edges and Nosetips

Paul Kolodziej, Ames Research Center, Moffett Field, California

July 1997

National Aeronautics and
Space Administration

Ames Research Center
Moffett Field, California 94035-1000

Nomenclature

A	reference area of vehicle, m^2
C_L	lift coefficient
$C_{N,2}, C_{O,2}$	concentration of atomic nitrogen or oxygen behind shock, J/kg
h	enthalpy, J/kg
h_D	dissociation enthalpy, J/kg
h_{RO_2}, h_{RN_2}	dissociation enthalpy of oxygen or nitrogen, J/kg
h_{ti}	total enthalpy, $h_i + V_i^2/2$, J/kg
Le	Lewis number = 1.4
m	vehicle mass, kg
M	Mach number
p	pressure, Pa
Pr	Prandtl number = 0.71
q_{cond}	heat conducted into TPS material, W/cm^2
q_{cont}	aerothermodynamic heating rate in continuum flow, W/cm^2
q_{rare}	aerothermodynamic heating rate in rarefied flow, W/cm^2
q_w	net aerothermodynamic heating rate, W/cm^2
R_{eff}	effective radius, $2^n R_N$, m
Re_{t2}	Reynolds number, $2^n \rho_{t2} R_N \sqrt{h_{t2}} / \mu_{t2}$
R_N	radius of leading edge or nosetip, m
R_0	planetary radius (6370 km for Earth)
T	temperature, K
T_{max}	maximum TPS temperature, K
V	velocity, m/s
V_s	surface grazing (circular) satellite speed (7.9 km/s)
X	$Log_{10}(Re_{t2})$
β	stagnation point velocity gradient, $\left[2(p_{t2} - p_1)/\rho_{t2}\right]^{1/2} / R_N$, 1/s

γ	ratio of specific heats
ε	density ratio across shock, ρ_1/ρ_2
ε_{TH}	total hemispherical emittance
λ_w	mean free path at body, $4(T_w/T_\infty)^{1/2} \lambda_\infty / (M_\infty \sqrt{\gamma\pi})$, m
λ_∞	mean free path at freestream, m
λ_2	mean free path behind shock, $(\rho_\infty/\rho_2)\lambda_\infty$, m
μ	dynamic viscosity, kg/m-s
ρ	density, kg/m^3
σ	Stefan Boltzman constant, 5.729E-8 w/m^2-K^4

Subscripts

$t1$	total conditions, freestream
$t2$	total conditions, behind shock
w	wall
1 or ∞	freestream
2	behind shock

Superscript

n	$n = 0$ for nosetip, $n = 1$ for unswept wing leading edge

Acronyms

CFD	computational fluid dynamics
FCCW	fully catalytic cold wall
FCHW	fully catalytic hot wall
FCRF	fully catalytic hot wall with rarefied flow effects
NCHW	noncatalytic hot wall
RLV	reusable launch vehicle
TPS	thermal protection system
UHTC	ultrahigh temperature ceramic

Aerothermal Performance Constraints for Hypervelocity Small Radius Unswept Leading Edges and Nosetips

PAUL KOLODZIEJ

Ames Research Center

Summary

Small radius leading edges and nosetips were utilized to minimize wave drag in early hypervelocity vehicle concepts until further analysis demonstrated that extreme aerothermodynamic heating would cause severe ablation or blunting of the available thermal protection system materials. Recent studies indicate that ultrahigh temperature ceramic (UHTC) materials are shape stable at temperatures approaching 3033 K and will be available for use as sharp UHTC leading edge components in the near future. Aerothermal performance constraints for sharp components made from these materials are presented in this work to demonstrate the effects of convective blocking, surface catalycity, surface emissivity, and rarefied flow effects on steady state operation at altitudes from sea level to 90 km. These components are capable of steady state operation at velocities up to 7.9 km/s at altitudes near 90 km.

Introduction

One of the strongest constraints in the design of a hypervelocity vehicle is the limit imposed by aerothermodynamic heating of a reusable thermal protection system (TPS). In extreme situations, exceeding the limits of the TPS will cause failure by ablation which may affect the vehicle aerodynamics and ultimately jeopardize the mission. In the early days of space flight, before guidance navigation and control were digital technologies, the accuracy of directing a vehicle through a critical entry corridor was not well established. Given these uncertainties, Chapman (ref. 1) suggested that it was "highly desirable to develop versatile protection shields for spacecraft which can radiate efficiently if entry happens to occur near overshoot, ablate efficiently if near undershoot, and blend these characteristics if entry occurs in between." Current TPS materials on the Shuttle possess these characteristics. Under normal operation they have an expected service of 50 flights but under severe operation begin to ablate or fail in a noncatastrophic manner.

Concurrently with the development of advanced TPS materials to meet the goals specified for the Shuttle,

knowledge of aerothermodynamic heating also advanced through arcjet studies, Shuttle flight experiments, and numerical analysis (refs. 2–4). The noncatalytic, high temperature behavior of ceramic TPS observed in these studies and those of other investigators indicates that significant improvements in the aerothermal performance constraint on hypervelocity vehicles may be possible. Although this information has been available, some trade studies still use fully catalytic, cold wall aerothermodynamic heating estimates of TPS material performance. This conservative approach may be constraining the trade studies to an area of the hypervelocity design space that does not contain the optimum concept for the current technology readiness level (ref. 5). A more aggressive but not necessarily higher risk design philosophy takes advantage of noncatalytic hot wall aerothermodynamic heating during the trade studies.

To illustrate the impact of noncatalytic, high temperature TPS materials on the hypervelocity design space for vehicle concepts, this work presents several examples of aerothermal performance constraints for small radius unswept leading edges and nosetips. These performance constraints are constructed on plots of altitude versus velocity in order to show the TPS material constraint on a vehicle's trajectory. Similar performance constraints can be constructed for any TPS material and vehicle geometry using this approach. By superimposing a trajectory on this type of plot, a vehicle designer can quickly determine whether the concept exceeds the limits of the TPS material.

Approach

Large variations in local aerothermodynamic heating rates commonly found on hypervelocity vehicles are due to the complex characteristics of the flow field. Today, advanced computational fluid dynamics (CFD) technologies are capable of "nose to tail" simulations that provide a three-dimensional view of localized heating (ref. 6). Before advanced CFD became available, a vehicle would be divided into components representing all of the key features: a nosetip, a wing leading edge, or a body panel at some incident angle to the freestream, etc., and the

local heating rates were calculated from appropriate engineering correlations. Generally, the results of both approaches show good agreement except where complex flow interactions exist, such as those found near the intersection of the fuselage and wing root. Although CFD provides better estimates for complex environments, CFD is too expensive for vehicle concept studies at this time. It is more productive to use accurate engineering correlations for perturbing the hypervelocity design space when performing trade studies which lead to optimized hypervelocity vehicles (ref. 7).

Laminar Stagnation Point Heating

Reusable TPS materials, like any other material, begin to fail at temperatures above their operating limits. A summary of the temperature limits (T_{max}) for both single use and multiple use applications of reusable ceramic TPS materials is contained in the TPSX database (ref. 8). Since these materials are good insulators and reradiate efficiently, a simple surface energy balance can be used to relate temperature to aerothermodynamic heating rate.

$$q_w - q_{cond} = \sigma \varepsilon_{TH} T_w^4 \qquad (1)$$

or

$$T_w = \left[(q_w - q_{cond})/\sigma \varepsilon_{TH} \right]^{1/4} \qquad (2)$$

For good insulators $q_{cond} \ll q_w$, and equation (2) can be simplified to a form commonly known as the equilibrium reradiated wall temperature.

$$T_w = \left(q_w / \sigma \varepsilon_{TH} \right)^{1/4} \qquad (3)$$

For laminar stagnation point heating rates on a hemispherical nose or unswept wing leading edge, the aerothermodynamic heating rate can be determined from an engineering correlation like the Fay and Riddell expression shown below (ref. 9). Similar engineering correlations can be found for the other components of a hypervelocity vehicle and aerothermodynamic heating effects, such as angle of attack, turbulence, shock impingement, or wake flow (refs. 10 and 11).

$$q_w = \frac{0.67}{\mathrm{Pr}} \left(\rho_w \mu_w \right)^{0.1} \left(\rho_{t2} \mu_{t2} \right)^{0.4}$$
$$\times \left\{ 1 + \left(\mathrm{Le}^{0.52} - 1 \right) \left(\frac{h_D}{h_{t2}} \right) \right\} \left\{ h_{t2} - h_w \right\} \left(\frac{\beta}{2^n} \right)^{1/2} \qquad (4)$$

At low velocities q_w is small and $T_w < T_{max}$, whereas at high velocities q_w is large and $T_w > T_{max}$, causing failure. By iterating on velocity in this manner until $T_w = T_{max}$, an aerothermal performance constraint can be constructed

like that shown in figure 1 for a two-dimensional, unswept leading edge having a 0.762 mm (0.03 in.) radius with a reusable leading edge temperature of 2149°C (3900°F) and surface emissivity of 80%. This geometry and the material conditions correspond to an earlier study on small radius leading edges for hypervelocity vehicles by Hill (ref. 12).

Algorithm Description

A brief description is presented of the Microsoft Excel macro that was developed to calculate aerothermodynamic heating for a given geometry as a function of altitude and velocity. To initiate the iterative solution, an altitude is chosen between 0 and 90 km. Freestream properties at this altitude are calculated from curve fits of physical properties given in the 1962 U.S. standard atmosphere (ref. 13). Next, an initial velocity slightly greater than $M_\infty = 1$ is chosen to calculate the conditions behind a shock from the Rankine-Hugoniot relations (ref. 14).

$$\left. \begin{array}{l} \rho_1 V_1 = \rho_2 V_2 \\[4pt] p_1 + \rho_1 V_1^2 = p_2 + \rho_2 V_2^2 \\[4pt] \tfrac{1}{2} V_1^2 + h_1 = \tfrac{1}{2} V_2^2 + h_2 \end{array} \right\} \qquad (5)$$

Starting with these normal shock conditions, the total pressure behind the shock p_{t2} is determined by isentropically compressing the gas until $h_2 = h_{t1}$. From the total properties p_{t2}, h_{t2} and the wall temperature T_{max}, the parameters $(\rho_{t2}, \mu_{t2}, \rho_w, \mu_w, h_w)$ for equation (4) can be determined and used for calculating q_w and T_w. Equilibrium properties of air are determined from the curve fits by Srinivasan (ref. 15). The dynamic viscosity of equilibrium air as a function of temperature is determined from the curve fits by Keyes (ref. 16).

Wall Conditions

Boundary conditions at the wall define the interaction (or couple), which is the TPS material response to the aerothermodynamic heating. By combining equations (3) and (4) it is possible to determine aerothermal performance constraints for multiple use and single use temperatures of TPS materials. Multiple use temperatures define the maximum temperature a material can withstand without significant degradation in performance or material properties. Single use temperatures are usually higher and define the minimum temperature at which a material will "fail," or no longer perform properly. It is important to recognize that more than one aerothermal performance constraint can be found for a material use

temperature because of the fluid/solid interaction effects on aerothermodynamic heating. To illustrate, figure 1 shows four examples that correspond to the following wall conditions:

1. Fully catalytic cold wall (FCCW)

2. Fully catalytic hot wall (FCHW)

3. Noncatalytic hot wall (NCHW)

4. Fully catalytic hot wall with rarefied flow effects (FCRF)

The most conservative limit shown at the lowest velocities in figure 1 is determined by calculating aerothermodynamic heating using a condition which is known as fully catalytic cold wall (FCCW) heating. FCCW heating is obtained by setting $h_w = 0$ and is most appropriate for an actively cooled metallic TPS.

The next limit to the right (at slightly higher velocities) is given by a less conservative condition at the wall which is known as fully catalytic hot wall (FCHW) heating. FCHW heating is obtained by setting h_w to the equilibrium enthalpy of air at p_{t2}, T_w and is most appropriate for a very clean, well insulated, hot metallic TPS. For comparison, the results from figure 1 of reference 12 are shown in table 1 along with the FCHW heating from figure 1 of this study.

Table 1. Aerothermal performance of the small radius unswept leading edge at low altitude

Altitude, km	Velocity, km/s (Present)	Velocity, km/s (Hill)
0	2.30	2.25
30	2.53	2.56

The next limit to the right is known as noncatalytic hot wall (NCHW) heating and is obtained by setting Le = 0 (see ref. 9). At hypervelocity, the strong shock wave dissociates the air molecules into atoms but causes little ionization. The enthalpy of dissociation h_D is given by

$$h_D = h_{RO_2} C_{O,2} + h_{RN_2} C_{N,2} \qquad (6)$$

and represents the chemical energy stored by the molecular dissociation behind the shock. On fully catalytic TPS materials, h_D is released by atomic recombination at the surface; it is not released on noncatalytic TPS materials. The catalytic behavior of reusable ceramic TPS materials listed in TPSX lies between these two limits and can be determined by using a more detailed approach like Goulard's (ref. 17). Atomic specie concentrations in this work were determined from curve fits of
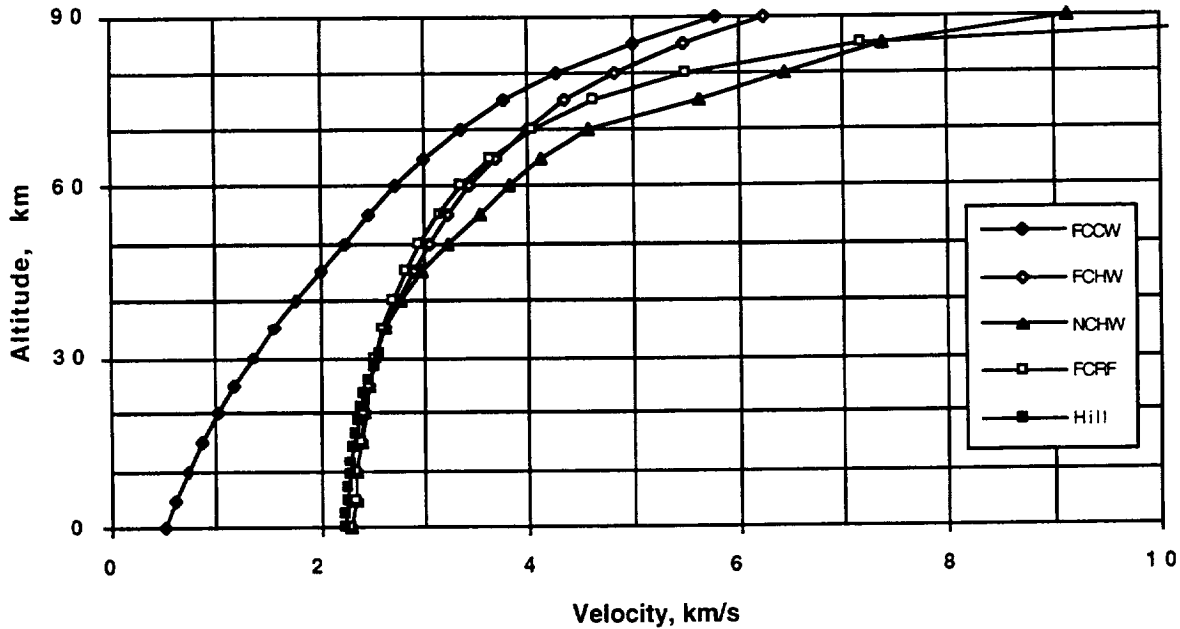

Figure 1. Aerothermal performance constraint (2-D stagnation point, $R_N = 0.76$ mm, $T_{max} = 2149°C$, $\varepsilon_{TH} = 80\%$).

Moeckell's results at the equilibrium air conditions behind the shock specified by ρ_2, T_2 (ref. 18).

The last limit to be discussed is known as fully catalytic hot wall heating with rarefied flow effects (FCRF) and is obtained by correcting q_w using a least squares fit of the experimental data compiled by Cheng (ref. 19) given by equation (7).

$$\frac{q_{rare}}{q_{cont}} = a_0 + a_1 X + a_2 X^2 + a_3 X^3 + a_4 X^4 + a_5 X^5 \quad (7)$$

$$a_0 \quad -1.38151$$

$$a_1 \quad +2.26375$$

$$a_2 \quad -0.54005$$

$$a_3 \quad -0.02164$$

$$a_4 \quad +0.02016$$

$$a_5 \quad -0.00170$$

Rarefied flow effects on aerothermodynamic heating are shown in figure 2. At high Reynolds numbers ($Re_{t2} > 10^5$) the stagnation region is characterized by a strong shock wave and thin boundary layer, where $q_{rare}/q_{cont} = 1$, and aerothermodynamic heating is given by a continuum expression like equation (4). As the Reynolds number decreases, the stagnation region begins a gradual transition to rarefied flow, and the effects on aerothermodynamic heating are given by applying equation (7) to equation (4).

The relationship shown in figure 2 depends on the interaction of several flow phenomena which occur as the Reynolds number decreases. As the Reynolds number decreases below $Re_{t2} = 10^5$, the thin boundary layer grows out toward the strong shock wave which increases heat conduction and $q_{rare}/q_{cont} > 1$. After reaching a maximum of $q_{rare}/q_{cont} = 1.19$ at $Re_{t2} = 534$, the shock wave begins to weaken and form a fully merged layer with the freestream which decreases heat conduction and q_{rare}/q_{cont}. When $Re_{t2} < 64$, the flow field has a smooth uniform behavior with no appearance of a shock-like structure and $q_{rare}/q_{cont} < 1$. For $Re_{t2} < 5.55$, the correlation is no longer valid and aerothermodynamic heating should be calculated from free collision theory.
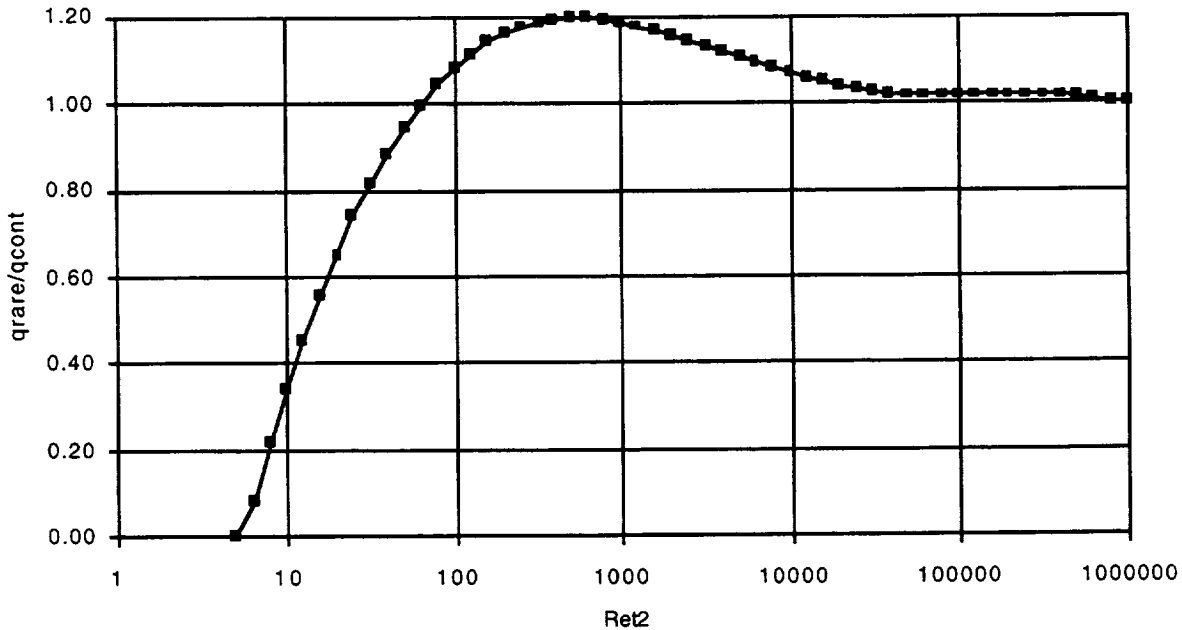

Figure 2. Rarefied flow effects on aerothermodynamic heating to the stagnation point of a hemisphere.

Results

Early hypervelocity vehicle concepts were based on extrapolations of the knowledge and experience acquired in the development of supersonic aircraft and, not surprisingly, led to vehicles that were slender bodies with sharp leading edges to produce weak shock waves and to minimize the wave drag (ref. 20). At hypervelocity, however, aerothermodynamic heating is severe, and sharp leading edges will naturally blunt by ablation to a larger radius. With this observation, Allen (ref. 21) developed an analysis showing that a blunt body significantly reduces aerothermodynamic heating by transferring the vehicle's kinetic energy to the atmosphere, or air behind the strong bow shock, instead of the TPS. In a short time, the leading edges on hypervelocity vehicles were blunted to reduce heating and minimize the amount of ablation.

Because of the aerodynamic advantages, it is important to reexamine the feasibility of hypervelocity vehicles with sharp leading edges for operation as commercial reusable launch vehicles (RLVs). Although shape stable, or nonablating, sharp leading edge components have been recognized as an important technology for implementing sharp body RLV concepts, the research and development effort has focused primarily on active cooling technologies. Impeding the implementation of actively cooled sharp leading edges on RLV are the high life-cycle costs required to guarantee that it works perfectly every

mission or fails in a noncatastrophic manner. Passive, nonablating sharp leading edge components which do not require such certification will inherently have a lower life-cycle cost.

From this perspective, an enabling technology for sharp body RLV concepts are the ceramic UHTC materials, such as the zirconium and hafnium diboride composites, currently under development by the Thermal Protection Materials and Systems Branch at Ames Research Center (ref. 22). UHTCs have a unique combination of mechanical, thermal, and chemical properties that enable the fabrication of very small radius or sharp leading edges for operation at hypervelocity. To efficiently implement passive, nonablating sharp leading edge UHTC components, it is necessary to understand the thermal structural behavior of these materials in order to fabricate components and to determine the nonablating aerothermal performance constraint on the flight envelope of altitude versus velocity.

The aerothermal performance constraint for a two-dimensional, unswept leading edge having a 1 mm radius with a single use temperature of 2760°C and surface emissivity of 80% is shown in figure 3. All of the limits in figure 1 have shifted to higher velocities in figure 3 because of the larger radius and increased temperature.
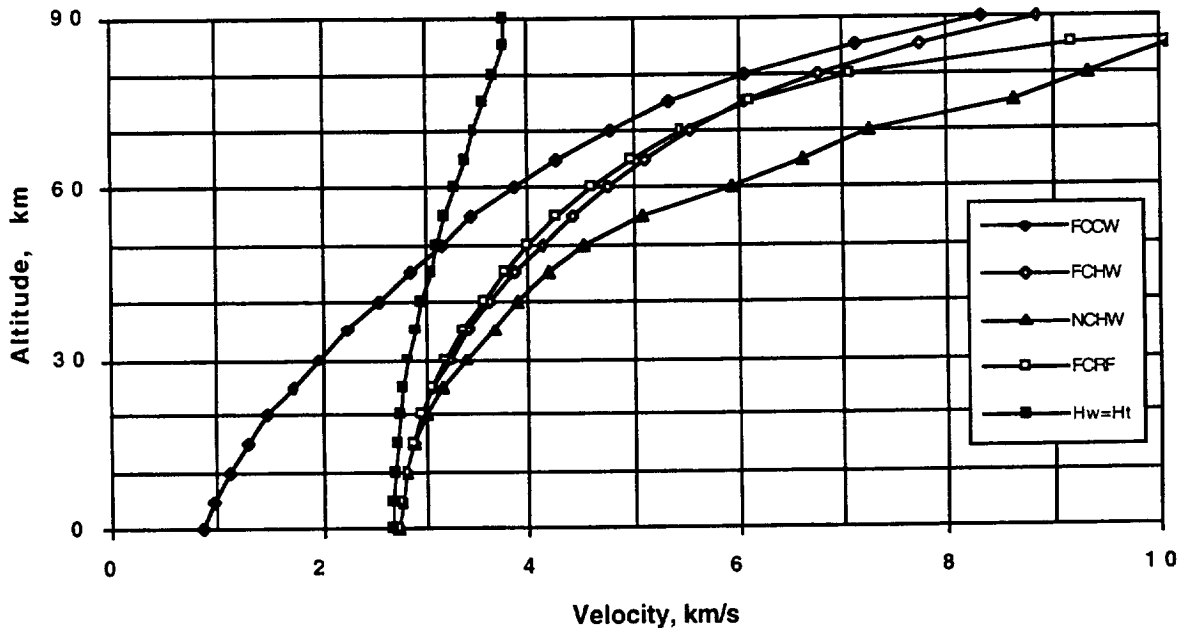

Figure 3. Aerothermal performance constraint (2-D stagnation point, $R_N = 1$ mm, $T_{max} = 2760°C$, $\varepsilon_{TH} = 80\%$).

Along with the limits shown in figure 1, another limit has been added to figure 3 identifying the conditions when complete convective blocking ($h_w = h_{t2}$) occurs. The importance of convective blocking, noncatalytic materials, surface emissivity, rarefied flow effects, transient heating, and material conduction on this TPS aerothermal performance constraint is discussed below.

Convective Blocking

Aerothermodynamic heating of very high temperature TPS materials is significantly reduced, or convectively blocked, when the wall enthalpy h_w is a significant fraction of the total enthalpy h_{t2}. With no convective blocking ($h_w = 0$) a TPS material will only operate up to the velocities shown by the cold wall (FCCW) limit in figure 3. Partial convective blocking enables operation at the velocities shown by the hot wall (FCHW) limit in figure 3 and is most effective at low altitude when h_{t2} is small. At high altitude, the velocity (h_{t2}) is much greater than h_w and convective blocking is much less effective. At a given altitude the importance of convective blocking is inversely proportional to the velocity difference between the FCCW and FCHW limits. With complete convective blocking ($h_w = h_{t2}$) no aerothermodynamic heating occurs. Under most circumstances, a TPS material operates at conditions to the right of the $h_w = h_{t2}$ limit where $h_w < h_{t2}$ and the surface is heated. Under circumstances where $h_w > h_{t2}$ the surface is cooled.

Noncatalytic Materials

Aerothermodynamic heating of noncatalytic TPS materials is significantly reduced when atoms dissociated by the shock are not recombined on the surface. All TPS materials defined by these material conditions ($T_{max} = 2760°C$, $\varepsilon_N = 80\%$) operate between the limits shown in figure 3 for a noncatalytic material (NCHW) and a fully catalytic material (FCHW). At very low altitudes in figure 3, little molecular dissociation occurs because of the high pressure behind the shock, and NCHW heating equals FCHW heating. Above 20 km, when dissociation begins to occur, a noncatalytic TPS material will operate at higher velocities (NCHW) than a catalytic TPS material (FCHW). Although this trend continues at higher altitudes as the velocity and dissociation increase, it is important to recognize that atomic recombination in the boundary layer may occur and the NCHW limit shifts back toward the FCHW limit. Also,

it is important to recognize that at very high altitudes rarefied flow effects sufficiently weaken the shock such that dissociation slows to produce few atoms and the NCHW limit shifts back toward the FCHW limit. Sophisticated CFD technologies with kinetically controlled reaction models of air are capable of accurately determining the secondary effects of these two phenomena.

For comparison, Goulard's (ref. 17) analysis of an axisymmetric hemispherical nose having a radius of 1.0 m for a wall temperature of 427°C (700 K) at 61 km (200 kft) is shown in figure 4 along with the ratio NCHW/FCHW from the present study at these conditions. Slight differences in figure 4 are due to property variations in the thermodynamic air models used in each study.

Surface Emissivity

On reusable TPS materials the surface emissivity may change with time because of surface contamination, oxide formation, or coating delamination. To illustrate this effect, the aerothermal performance constraint shown in figure 3 with a surface emissivity of 80% has been duplicated in figure 5 for a surface emissivity of 40%. All of the limits in figure 3 shift to lower velocities, with the largest decrease occurring at high altitude. At low altitude, where convective blocking of very high temperature TPS materials is most effective, surface emissivity has little effect on velocity. In general, TPS materials with low emissivity operate closer to the $h_w = h_{t2}$ limit where convective blocking is more effective.

Rarefied Flow Effects

Aerothermodynamic heating of sharp wing leading edges or nosetips is significantly reduced when the Reynolds number Re_{t2} is low and the stagnation region flow becomes rarefied. To illustrate this effect, the aerothermal performance constraint shown in figure 5 for an unswept wing leading edge has been duplicated in figure 6 for a three-dimensional nosetip at zero angle of attack. All of the limits in figure 5 shift to lower velocities, with the largest decrease occurring at high altitude. As expected, the FCRF limit in figure 6 is almost identical with the FCHW limit at low altitude (high Re_{t2}) and begins to shift to higher velocities at high altitude (low Re_{t2}) as rarefied flow effects become significant.
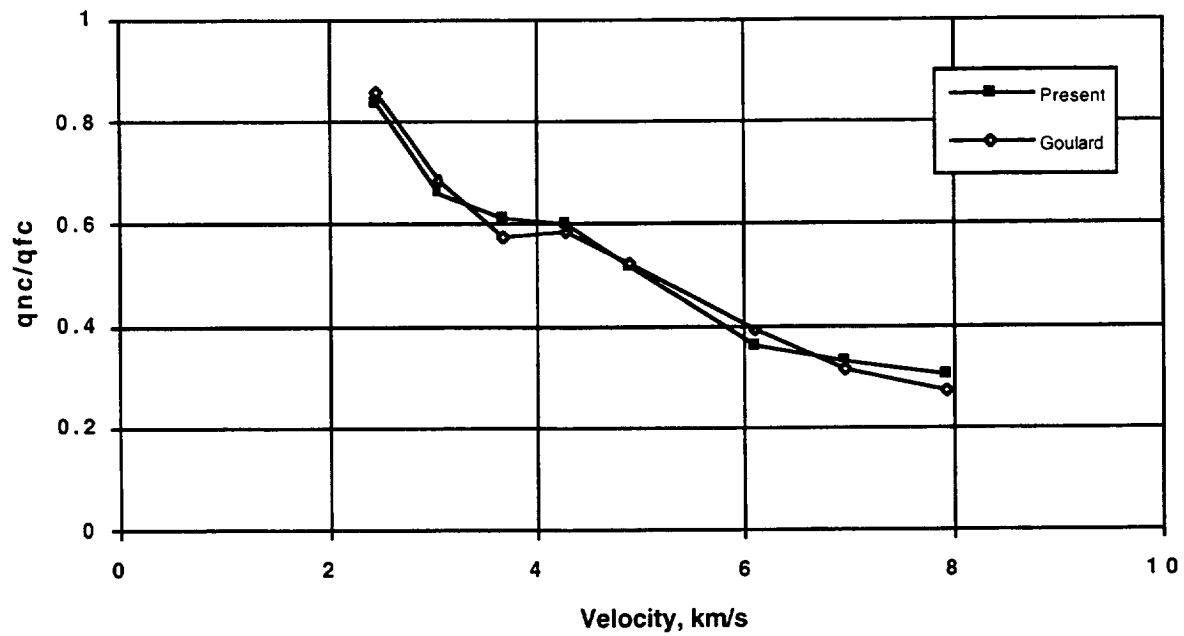
6

Figure 4. Reduced aerothermodynamic heating to a noncatalytic surface at 61 km.
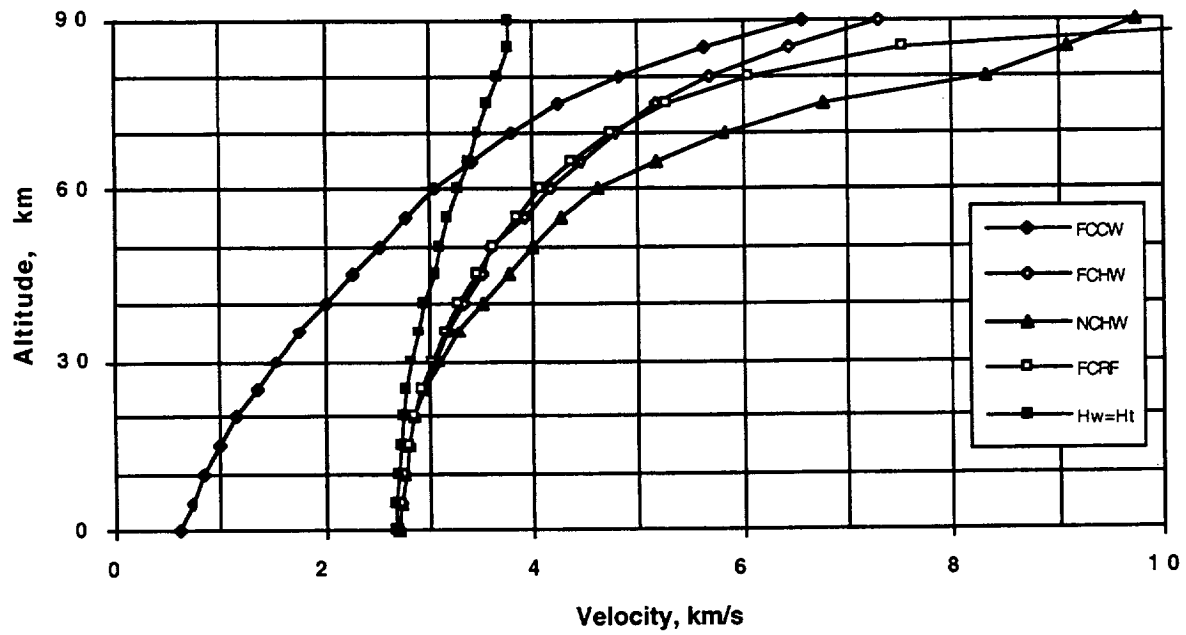

Figure 5. Surface emissivity effects (2-D stagnation point, $R_N = 1$ mm, $T_{max} = 2760°C$, $\varepsilon_{TH} = 40\%$).
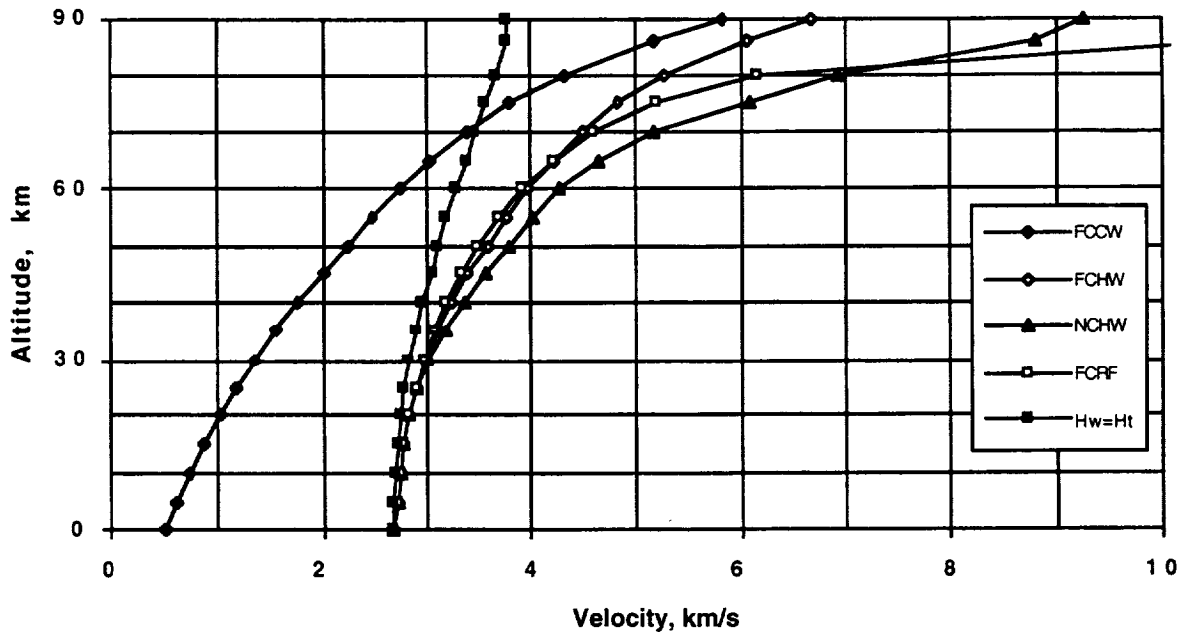
Figure 6. Rarefied flow effects (3-D stagnation point, $R_N = 1$ mm, $T_{max} = 2760°C$, $\mathcal{E}_{TH} = 40\%$).

Near 90 km, sharp geometries operate up to velocities given by the FCRF limit and exceed the velocities given by the NCHW limit. Because molecular dissociation decreases as the shock weakens at low Re_{t2} (near 90 km in this case) and $h_D \to 0$, both the FCHW and NCHW limits converge (refs. 23 and 24).

These effects are confined to the stagnation region of a sharp leading edge or a nosetip. Downstream of this region the flow begins a natural transition to continuum flow, and conventional aerothermodynamic correlations like equation (4) still apply.

The transition from rarefied flow to continuum flow is normally classified into flow regimes having common characteristics using a Knudson number defined as a ratio of the mean free path (air) to a characteristic length of the sharp leading edge or nosetip (radius) (ref. 25). Probstein's criteria for this type of detailed classification on a cold sphere having a 0.3048 m radius are shown in figure 1 of reference 25. These criteria, their corresponding altitudes at 7.9 km/s, and the corresponding Re_{t2}

values are listed in table 2. An alternate method for classifying flow regimes is possible using Re_{t2} values that correspond to Probstein's criteria.

Transient Effects and Conduction

All of the limits in the aerothermal performance constraint shift to higher velocities by transient effects and heat conduction into the material. Transient effects will shift the limits to higher velocities at the beginning of entry when the TPS material is cold. As the surface temperature approaches steady state, the TPS material must be operated at velocities close to the appropriate limit. At lower altitudes, the limits will still be shifted to higher velocities because the aerothermodynamic heating is changing continuously as the vehicle maneuvers and the TPS material never reaches the steady state temperatures used to calculate these performance constraints. Heat conduction into the TPS material reduces T_w (see eq. (2)) and enables higher velocities.

8

Table 2. Rarefied gas flow regimes for the stagnation region of a hemisphere ($R_N = 0.3048$ m)

Flow regime transition	Criteria	Altitude, km (Probstein)	Re_{t2}
Free molecule → First collision	$\lambda_w = 10 R_{eff}$	147.7	n/a
First collision → Transitional layer	$\lambda_w = R_{eff}/3$	188.8	12
Transitional layer → Fully merged layer	$\lambda_2 = \varepsilon R_{eff}$	106.7	63
Fully merged layer → Incipient merged layer	$\lambda_2 = \varepsilon R_{eff}/10$	92.9	620
Incipient merged layer → Viscous layer	$\lambda_2 = \varepsilon^{3/2} R_{eff}/10$	83.9	2,932
Viscous layer → Vorticity interaction	$\lambda_2 = \varepsilon^2 R_{eff}/10$	75	12,385
Vorticity interaction → Boundary layer	$\lambda_\infty = \varepsilon^2 R_{eff}/100$	59.8	78,926

Discussion

Entry from low Earth orbit at 7.9 km/s along trajectories that coincide with TPS aerothermal performance constraints (corresponding to the maximum temperature of the TPS material) have the shortest duration and are known as minimum heat load trajectories (ref. 26). Few vehicles fly these trajectories to landing because of G-load (gravity-load) constraints on humans and/or the structure, but instead transition from the minimum heat-load constraint to the G-load constraint. The time from initial entry to landing along the actual trajectory path and the local transient aerothermodynamic heating rates are required in order to estimate the TPS thickness for insulating the structure and hence the total weight of the TPS subsystem. Both downrange and cross-range maneuvering can add substantial time to the entry trajectory, increasing the integrated heat load and hence the TPS thickness and weight.

To illustrate minimum heat load trajectories, the aerothermal performance constraint shown in figure 6 has been duplicated in figure 7 for a 1 cm radius. All of the limits in figure 6 have shifted to higher velocities because of the larger radius. The G-load constraint added to figure 7 is defined by an equilibrium glide path with $m/C_L A = 1750$ kg/m^2 using

$$\rho_1 = \frac{2}{R_0}\left(\frac{m}{C_L A}\right)\left(\frac{V_s^2}{V_1^2} - 1\right) \qquad (8)$$

Altitude is related to velocity along this constraint by first selecting an altitude to calculate ρ_1 from the 1962 standard atmosphere and then determining V_1 (ref. 27). It coincides with the NCHW limit down to 50 km and

then decelerates more rapidly at lower altitudes. An optimum trajectory follows the NCHW limit down to 50 km, then transitions to follow the G-load limit to landing.

In general, selection of an entry trajectory depends on the experience of the vehicle designer. If the designer is not familiar with TPS materials and employs the conservative FCHW limit, the equilibrium glide path to be used in landing will be limited to $m/C_L A < 250$ kg/m^2. An even more conservative approach using the FCCW limit constrains the equilibrium glide path to $m/C_L A < 150$ kg/m^2. Achieving low values of $m/C_L A$ may be accomplished by decreasing the mass or increasing the lift; either strategy is difficult and expensive. High values of $m/C_L A$ are less difficult and expensive to design, fabricate, and operate.

For sharp geometries ($R_N = 1$ mm; see fig. 6), a third approach follows the FCRF limit until the rarefied flow effects that lower aerothermodynamic heating begin to subside, then transitions to the NCHW, and finally transitions to the G-load limit for landing. A more detailed analysis is required to determine the relationship between these approaches and the TPS system weight.

It is important to recognize that the asymptotic behavior of the FCRF limit indicates sharp leading edge vehicles may be operated at very high velocities ($V > 10$ km/s) above 90 km. This limit may be useful in designing lunar or planetary return missions which slow down by aerobraking or aerocapture maneuvers at high altitude without ablation in order to minimize the uncertainty in guidance, navigation, and control. When operating along the FCRF limit during these maneuvers the aerothermodynamic
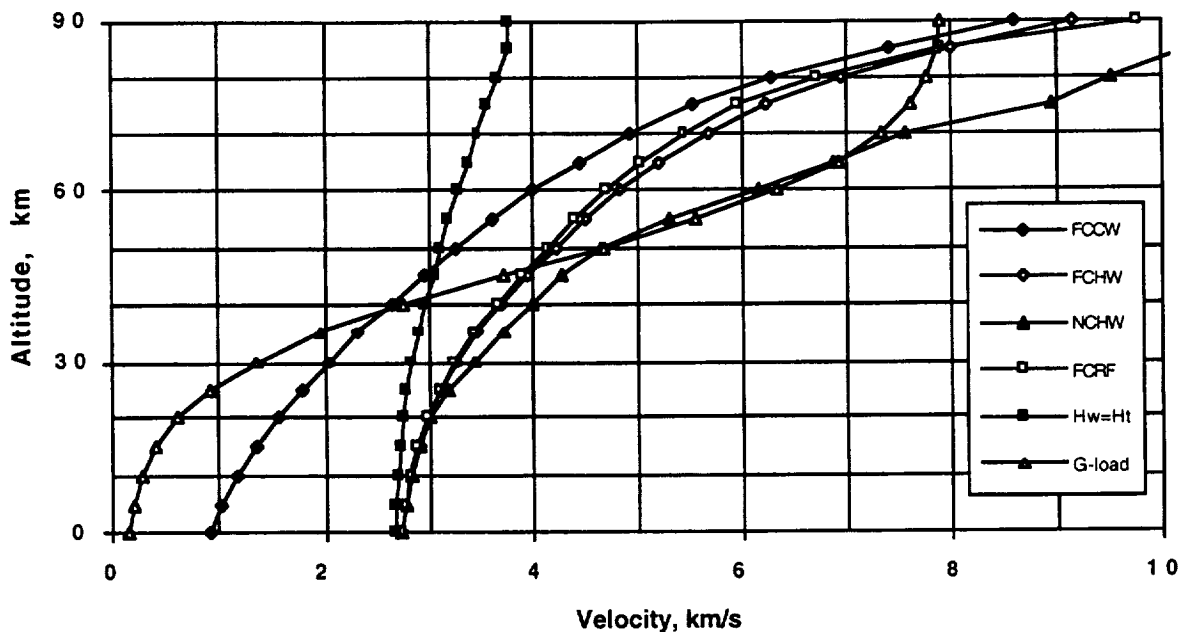
Figure 7. Aerothermal performance constraint (3-D stagnation point, $R_N = 1$ cm, $T_{max} = 2760°C$, $\varepsilon_{TH} = 40\%$).

heating of the aftbody TPS material behind the non-ablating sharp leading edge gradually transitions from rarefied to continuum flow. The selection, sizing, and design of the aftbody TPS materials for these missions may be more challenging than the sharp leading edge design.

Experimental measurements of steady state rarefied flow effects on the aerothermodynamic heating of ultrahigh temperature TPS materials are not available. Currently, most measurements of hypervelocity behavior are conducted in continuous flow facilities like arcjets or pulse flow facilities like shock tunnels. TPS material evaluation studies are usually conducted in arcjets for long duration (minutes) in order to establish the steady state use temperatures in TPSX. At this time, the measurement of rarefied flow effects is limited to moderate Reynolds numbers in the high temperature dissociated freestream flow of arcjet facilities. Although shock tunnels operate at lower Reynolds numbers, the exposure time (milliseconds) is too short for accurate measurements of the TPS material response.

Flight experiments would provide the correct environment for measuring these effects and benchmarking either engineering correlations or CFD analysis. Transient measurements can be made by flying a sharp leading edge or nosetip on any of several existing sounding rockets,

similar to early studies of aerothermodynamics (ref. 28). A more precise experimental measurement can be made using a downward-deployed tethered platform as described by Wood (ref. 29). A sharp diboride nosetip, or leading edge, downward-deployed to 90 km at 7.9 km/s would provide steady state measurements of aerothermodynamic heating at the top of the FCRF limit.

Conclusion

Aerothermal performance constraints based on aerothermodynamic heating correlations for hypervelocity vehicle components provide the designer with a rapid technique for evaluating how close new vehicle concepts approach the temperature failure limit of TPS materials. These constraints show that aerothermodynamic heating of sharp leading edges and nosetips is significantly reduced at high altitude by noncatalytic and rarefied flow effects which shift the TPS performance limit to velocities greater than 7.9 km/s at 90 km. Sharp body concepts using small radius leading edges or nosetips have lower wave drag than blunt body concepts and may be suitable for single stage to orbit concepts, long duration ascent of RLV concepts, or the extended range entry of waverider concepts.

10

References

1. Chapman, D. R.: An Analysis of the Corridor and Guidance Requirements for Supercircular Entry into Planetary Atmospheres. NASA TR R-55, 1960.

2. Pope, R. B.: Stagnation-Point Convective Heat Transfer in Frozen Boundary Layers. AIAA J., vol. 6, no. 4, Apr. 1968, pp. 619–626.

3. Stewart, D. A.; Rakich, J. V.; and Lanfranco, M. J.: Catalytic Surface Effects on Space Shuttle Thermal Protection System during Earth Entry of Flights STS-2 through STS-5, Shuttle Performance: Lessons Learned. NASA CP-2283, Part 2, 1983.

4. Stewart, D. A.; Rakich, J. V.; and Chen, Y. K.: Flight Experiment Demonstrating the Effect of Surface Catalysis on the Heating Distribution over the Space Shuttle Heat Shield. Orbiter Experiments Aerothermodynamics Symposium, NASA Langley Research Center, Williamsburg, Va., Apr. 1993.

5. Access to Space, Advanced Technology Team, Final Report. Vol. 3. NASA, July 1993.

6. Edwards, T. A.; and Flores, J.: Computational Fluid Dynamics Nose-to-Tail Capability: Hypersonic Unsteady Navier-Stokes Code Validation. J. Spacecraft and Rockets, vol. 27, no. 2, Mar./Apr. 1990, pp. 123–130.

7. Thompson, R. A.; and Riley, C. J.: Engineering Code for Hypersonic Vehicle Optimization. J. Spacecraft and Rockets, vol. 31, no. 1, Jan./Feb. 1994, pp. 150–152.

8. TPSX computer program, NASA Ames Research Center, Dec. 1994.

9. Fay, J. A.; and Riddell, F. R.: Theory of Stagnation Point Heat Transfer in Dissociated Air. J. Aeronaut. Sci., vol. 25, no. 2, Feb. 1958, pp. 54–67.

10. Hankey, W. L.; Neumann, R. D.; and Flinn, E. V.: Design Procedures for Computing Aerodynamic Heating at Hypersonic Speeds. WADC TR 59-610, June 1960.

11. Tauber, M. E.: A Review of High-Speed Convective, Heat-Transfer Computation Methods. NASA TP-2914, July 1989.

12. Hill, M. L.: Materials for Small Radius Leading Edges for Hypersonic Vehicles. J. Spacecraft and Rockets, vol. 5, no. 1, Jan. 1968, pp. 55–61.

13. U.S. Standard Atmosphere, 1962. U.S. Govt. Printing Office, Washington, D.C., Dec. 1962.

14. Equations, Tables, and Charts for Compressible Flow. NACA Report 1135, 1953.

15. Srinivasan, S.; Tannehill, J. C.; and Weilmuenster, K. J.: Simplified Curve Fits for the Thermodynamic Properties of Equilibrium Air. ISU-ERI-Ames-86401, June 1986.

16. Keyes, F. G.: A Summary of Viscosity and Heat-Conduction Data for He, A, H_2, O_2, N_2, CO_2, CO, H_2O and Air. Transactions of the ASME, vol. 73, no. 5, July 1951, pp. 589–596.

17. Goulard, R.: On Catalytic Recombination Rates in Hypersonic Stagnation Heat Transfer. ARS J., vol. 28, Nov. 1958, pp. 737–745.

18. Moeckel, W. E.; and Weston, K. C.: Composition and Thermodynamic Properties of Air in Chemical Equilibrium. NACA TN 4265, Feb. 1958.

19. Cheng, H. K.: The Blunt-Body Problem in Hypersonic Flow at Low Reynolds Number. Cornell Aeronautical Laboratory, CAL Report No. AF-1285-A-10, June 1963.

20. Anderson, J. D.: Hypersonic and High Temperature Gas Dynamics. McGraw-Hill, Inc., 1989, pp. 6–7.

21. Allen, H. J.; and Eggers, A. J., Jr.: A Study of the Motion and Aerodynamic Heating of Missiles Entering the Earth's Atmosphere at High Supersonic Speeds. NACA RM A53D28, Aug. 1953.

22. Bull, J. D.; Rasky, D. J.; Tran, H. K.; and Balter-Peterson, A.: Material Response of Diboride Matrix Composites to Low Pressure Simulated Hypersonic Flows. NASA CP-3235, Part 2, May 1994, pp. 653–673.

23. Chung, P. M.: Hypersonic Viscous Shock Layer of Nonequilibrium Dissociating Gas. NASA TR R-109, May 1961.

24. Inger, G. R.: Nonequilibrium Hypersonic Stagnation Flow with Arbitrary Surface Catalycity Including Low Reynolds Number Effects. Int. J. Heat Mass Transfer, vol. 9, 1966, pp. 755–772.

25. Probstein, R. F.: Shock Wave and Flow Field Development in Hypersonic Re-Entry. Amer. Roc. Soc., Paper 1110-60 presented at ARS Semi-Annual Meeting, Los Angeles, Calif., May 1960.

26. Havey, K. A.: Entry Vehicle Performance in Low-Heat Load Trajectories. J. Spacecraft and Rockets, vol. 19, no. 6, Nov./Dec. 1982, pp. 506–512.

27. Tauber, M. E.; and Yang, L.: Performance Comparisons of Maneuvering Vehicles Returning from Orbit. J. Spacecraft and Rockets, vol. 25, no. 4, July/Aug. 1988, pp. 263–270.

28. Chauvin, L. T.; and Speegle, K. C.: Boundary Layer Transition and Heat Transfer Measurements from Flight Tests of Blunt and Sharp 50 Cones at Mach Numbers from 1.7 to 4.7. NACA RM L57D04, Apr. 1957.

29. Wood, G. M.; Siemers, P. M.; Squires, R. K.; Wolf, H.; Carlomango, G. M.; and DeLuca, L.: Downward-Deployed Tethered Platforms for High-Enthalpy Aerothermodynamic Research. J. Spacecraft and Rockets, vol. 27, no. 2, Mar./Apr. 1990, pp. 216–221.

REPORT DOCUMENTATION PAGE

Public reporting burden for this collection of information is estimated to average 1 hour per response, including the time for reviewing instructions, searching existing data sources, gathering and maintaining the data needed, and completing and reviewing the collection of information. Send comments regarding this burden estimate or any other aspect of this collection of information, including suggestions for reducing this burden, to Washington Headquarters Services, Directorate for information Operations and Reports, 1215 Jefferson Davis Highway, Suite 1204, Arlington, VA 22202-4302, and to the Office of Management and Budget, Paperwork Reduction Project (0704-0188), Washington, DC 20503.

1. AGENCY USE ONLY *(Leave blank)*	2. REPORT DATE July 1997	3. REPORT TYPE AND DATES COVERED Technical Memorandum

4. TITLE AND SUBTITLE

Aerothermal Performance Constraints for Hypervelocity Small Radius Unswept Leading Edges and Nosetips

5. FUNDING NUMBERS

242-72-01

6. AUTHOR(S)

Paul Kolodziej

7. PERFORMING ORGANIZATION NAME(S) AND ADDRESS(ES)

Ames Research Center
Moffett Field, CA 94035-1000

8. PERFORMING ORGANIZATION REPORT NUMBER

A-976832

9. SPONSORING/MONITORING AGENCY NAME(S) AND ADDRESS(ES)

National Aeronautics and Space Administration
Washington, DC 20546-0001

10. SPONSORING/MONITORING AGENCY REPORT NUMBER

NASA TM-112204

11. SUPPLEMENTARY NOTES

Point of Contact: Paul Kolodziej, Ames Research Center, MS 234-1, Moffett Field, CA 94035-1000
(415) 604-0356

12a. DISTRIBUTION/AVAILABILITY STATEMENT

Unclassified — Unlimited
Subject Categories 18, 27

12b. DISTRIBUTION CODE

13. ABSTRACT *(Maximum 200 words)*

Small radius leading edges and nosetips were utilized to minimize wave drag in early hypervelocity vehicle concepts until further analysis demonstrated that extreme aerothermodynamic heating would cause severe ablation or blunting of the available thermal protection system materials. Recent studies indicate that ultrahigh temperature ceramic (UHTC) materials are shape stable at temperatures approaching 3033 K and will be available for use as sharp UHTC leading edge components in the near future. Aerothermal performance constraints for sharp components made from these materials are presented in this work to demonstrate the effects of convective blocking, surface catalycity, surface emissivity, and rarefied flow effects on steady state operation at altitudes from sea level to 90 km. These components are capable of steady state operation at velocities up to 7.9 km/s at altitudes near 90 km.

14. SUBJECT TERMS

Hypersonic, TPS, Aerothermodynamic heating, diboride materials, Small radius leading edge

15. NUMBER OF PAGES

16

16. PRICE CODE

A03

17. SECURITY CLASSIFICATION OF REPORT	18. SECURITY CLASSIFICATION OF THIS PAGE	19. SECURITY CLASSIFICATION OF ABSTRACT	20. LIMITATION OF ABSTRACT
Unclassified	Unclassified		